catalysts

MDPI

Article

Effect of Fe_2O_3–ZrO_2 Catalyst Morphology on Sulfamethazine Degradation in the Fenton-Like Reaction

Pan Gao *, Mengjie Hao, Yue He, Yuan Song and Shaoxia Yang *

National Engineering Laboratory for Biomass Power Generation Equipment, North China Electric Power University, Beijing 102206, China; haomengjie2018@163.com (M.H.); heyue61@163.com (Y.H.); songyuan_0601@163.com (Y.S.)

* Correspondence: gaopan@ncepu.edu.cn (P.G.); yangshaoxia@ncepu.edu.cn (S.Y.); Tel.: +86-106-177-2456 (S.Y.)

Received: 17 December 2018; Accepted: 9 January 2019; Published: 14 January 2019

Abstract: Fe_2O_3–ZrO_2 catalysts with different morphologies (nanoplates (HZNPs), nanorods (HZNRs), nanocubes (HZNCs), and nanotubes (HZNTs)) were prepared by a hydrothermal method to investigate the effect of the morphology on the catalytic performance in the Fenton-like reaction for sulfamethazine (SMT) degradation. The Fe_2O_3–ZrO_2 catalysts were characterized by scanning electron microscope (SEM), X-ray diffraction (XRD), X-ray photoelectron spectroscopy (XPS), and Brunauer–Emmett–Teller (BET) analysis. The H_2O_2 adsorption and the Fe^{2+} density sites on the Fe_2O_3–ZrO_2 catalysts had a close relationship with the morphologies and exhibited an important effect on the ·OH formation in the Fenton-like reaction. Free ·OH radicals were the main oxidative species in the reaction, and the normalized ·OH concentration per surface area of the catalysts was 4.52, 2.24, 2.20, and 0.37 μmol/m^2 for HZNPs, HZNRs, HZNCs, and HZNTs, respectively. The Fe_2O_3–ZrO_2 catalysts with different morphologies showed good catalytic performance, and the order of SMT degradation was HZNPs > HZNRs > HZNCs > HZNTs. Total SMT removal was achieved in the Fenton-like reaction over HZNPs at pH 3.0 and 45 °C after 240 min.

Keywords: Fenton-like reaction; hematite; structure-dependent reactivity; ZrO_2; sulfamethazine

1. Introduction

Advanced oxidation processes (AOPs), involving ozone, photocatalysis, electrochemical oxidation, Fenton reaction and wet air oxidation and so on, are efficient treatment technologies for degrading toxic and/or refractory organic compounds [1–4]. Among the AOPs, the Fenton reaction (Fe^{2+}/H_2O_2), as a green, simple and efficient process, can remove bio-refractory organic compounds. However, the application of the traditional Fenton reaction is limited in wastewater treatment, due to a narrow pH range and sludge production [2]. The heterogeneous Fenton-like process can avoid these shortcomings to some extent. Iron-based oxides (such as Fe_3O_4, Fe_2O_3, FeOOH, Fe^0, etc.), which are environmental-friendly and easily available materials, exhibit good performance in the heterogeneous Fenton-like reaction [3–8]. Compared to Fe_3O_4, hematite (α-Fe_2O_3) showed good chemical stability along with poor activity. The development of iron oxide catalysts with good activity and stability is a crucial challenge for the heterogeneous Fenton-like reaction.

The performance of heterogeneous catalysts not only depends on their chemical composition, size, and surface area but also on the morphology and arrangement manner of the surface atoms. Hematite with different morphologies (such as nanocubes, nanorods, nanobelts, nanoflowers, etc.) has been widely focused [9,10]. The literature shows that the morphology of α-Fe_2O_3 can affect the catalytic efficiency of the reactions [11,12]. For instance, Zhang et al. found that hematite nanorods with exposed {110} facets exhibited a better foreign ion confinement capacity (Fe^{2+}) and a higher H_2O_2

adsorption than hematite nanoplates with exposed {001} facets [13]. The result indicated that different morphologies of iron oxides could improve the catalytic activity in the Fenton-like reaction. Moreover, it was reported that the addition of transition metals (such as Ti^{4+}, Ce^{4+}, V^{4+}, Zr^{4+}, etc.) into iron oxides enhanced the catalytic activity in the Fenton-like reaction [14–16]. According to the above literature, we proposed a brand-new idea, synthesis of shape-controlled metallic oxides, for improving the performance of heterogeneous Fenton-like catalysts. Unfortunately, the effect of the different morphologies of bimetallic oxide catalysts on the catalytic performance has not been investigated in detail, and the reaction mechanism was not clearly in the heterogeneous Fenton-like system.

Sulfamethazine (SMT), one of the pharmaceutically active compounds (PhACs), is widely used due to its use simplicity, high chemical stability, good antimicrobial activity, fast absorption, and low price [1]. So the SMT is often detected in the aquatic environment, and selected as a target pollutant. In the study, we prepared the shape-controlled Fe_2O_3–ZrO_2 catalysts, evaluated the H_2O_2 adsorption/decomposition process to produce ·OH radicals, and investigated the effect of the morphology on the catalytic activity of the Fe_2O_3–ZrO_2 catalysts in the Fenton-like reaction for degrading SMT. Moreover, the reaction mechanism was proposed for the Fenton-like reaction over the shape-controlled Fe_2O_3–ZrO_2 catalysts.

2. Results and Discussions

2.1. Characterization of the Catalysts

2.1.1. Scanning Electron Microscope (SEM) Analysis

Figure 1 shows the morphologies of Fe_2O_3 and Fe_2O_3–ZrO_2 catalysts in the SEM images. Pure Fe_2O_3 with regular morphologies and sizes, involving nanoplates (HNPs), nanorods (HNRs), nanocubes (HNCs), and nanotubes (HNTs), was consistent with the literature [17,18]. Appropriate reagents (such as surfactant, additives, etc.) can affect the growth rate of various facets of Fe_2O_3 in the growth process [11,19]. Moreover, the addition of metal ions effectively retained the aggregation of the catalysts, and led to the formation of a crystal particle with a smaller size [16]. The above results indicated that the smaller particle and similar morphology could be obtained with the Zr addition, in good agreement with our study (in Figure 1). For the Fe_2O_3–ZrO_2 catalysts with different morphologies, the nanoplates (HZNPs) exhibited an irregular plate-like structure, and the diameter decreased from ca. 214 nm to ca. 143 nm; the nanorods (HZNRs) became like short and thick sticks, and the length was obviously reduced from ca. 695 nm to ca. 217 nm; the nanocubes (HZNCs) evolved from cube to olive-shaped with a smaller size; the nanotubes (HZNTs) gradually lost the shape of nanotubes and formed a wrinkled sheet-like structure.

2.1.2. X-Ray Diffraction (XRD) and Brunauer–Emmett-Teller (BET) Analysis

For the shape-controlled Fe_2O_3–ZrO_2 catalysts, the XRD patterns revealed that diffraction peaks of α-Fe_2O_3 with hexagonal crystal structure were observed, and weaker ZrO_2 diffraction peaks were also observed (in Figure 2). Compared with Fe_2O_3 (in Figure S1), the Zr addition weakened the intensity of α-Fe_2O_3 peaks, suggesting that the Zr addition inhibited the Fe_2O_3 agglomeration and reduced the Fe_2O_3 crystallite size. According to the Scherrer's equation, the crystallite sizes of α-Fe_2O_3 for HZNTs, HZNPs, HZNRs and HZNCs were 35, 47, 66, and 75 nm, respectively. As shown in Table 1, the surface areas for HZNTs, HZNPs, HZNRs, and HZNCs were 193, 107, 97, and 66 m^2/g, and obviously increased, compared with that of pure Fe_2O_3 (in Table S1). The result was consistent with that of SEM of the Fe_2O_3–ZrO_2 catalysts.

2.1.3. X-Ray Photoelectron Spectroscopy (XPS) Analysis

XPS analysis was used to characterize the chemical states of the shape-controlled Fe_2O_3–ZrO_2 catalysts. The Zr, O, and Fe peaks were observed at ca. 182, 530, and 711 eV, respectively (in Figure 3a). For pure Fe_2O_3, the Fe $2p_{3/2}$ peak appeared at 710.6 eV and was attributed to Fe^{3+}-O. With the Zr

addition, the binding energy of Fe $2p_{3/2}$ shifted from 710.6 to 710.1 eV (in Figure 3b), indicating that the chemical state of Fe element changed in the Fe_2O_3–ZrO_2 catalysts. The Fe $2p_{3/2}$ peaks were fitted into two peaks and assigned to Fe^{2+}-O (ca. 708.5 eV) and Fe^{3+}-O (ca. 710.6 eV) [20]. According to the fitting results, the different Fe^{2+} amounts for HNZPs, HNZRs, HNZCs, and HNZTs were 28, 18, 6, and 9 at. %, respectively. As iron oxides are used as catalysts in the Fenton-like reaction, Fe^{2+} favors the ·OH formation, and a high Fe^{2+} concentration is advantageous to improve the degradation of organic pollutants [16].

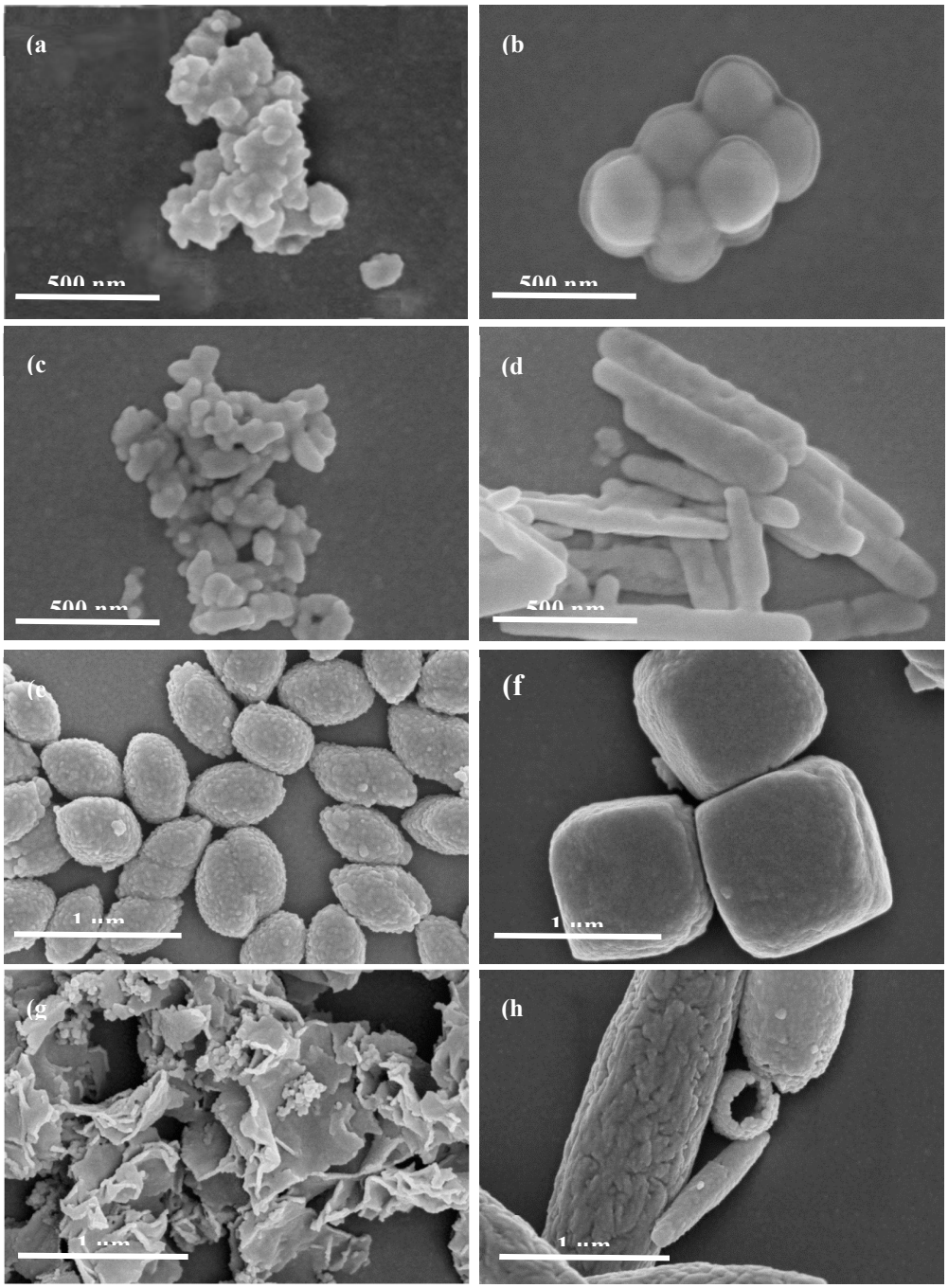

Figure 1. Scanning electron micsroscope (SEM) images on: (**a**) Fe_2O_3-ZrO_2 nanoplates (HZNPs), (**b**) Fe_2O_3 nanoplates (HNPs), (**c**) Fe_2O_3-ZrO_2 nanorods (HZNRs), (**d**) Fe_2O_3 nanorods (HNRs), (**e**) Fe_2O_3-ZrO_2 nanocubes (HZNCs), (**f**) Fe_2O_3 nanoplates (HNCs), (**g**) Fe_2O_3-ZrO_2 nanotubes (HZNTs), (**h**) Fe_2O_3 nanotubes (HNTs).

Table 1. Physicochemical properties of the shape-controlled Fe_2O_3–ZrO_2 catalysts.

Shape	d_{Fe} [nm]	Surface area [m^2/g]	ω_{Fe}[a] [wt.%]	SDIAs[b] [Fe/nm^2]	τ_{Fe2+}[c] [at.%]	Density site[d] [Fe^{2+}/nm^2]
HZNPs	47	107	0.21	21.10	0.28	5.91
HZNRs	66	97	0.26	28.81	0.18	5.18
HZNCs	75	66	0.25	40.72	0.06	2.44
HZNTs	35	193	0.19	10.03	0.09	0.90

[a] The mass ratio of Fe on the catalysts surface; [b] SDIAs = $\omega_{Fe} \times N_A/(SSA \times 56 \times 10^{18})$; [c] The atomic ratio of $Fe^{2+}/(Fe^{2+} + Fe^{3+})$ on the catalysts surface; [d] Density Site = SDIAs × τ_{Fe2+}.

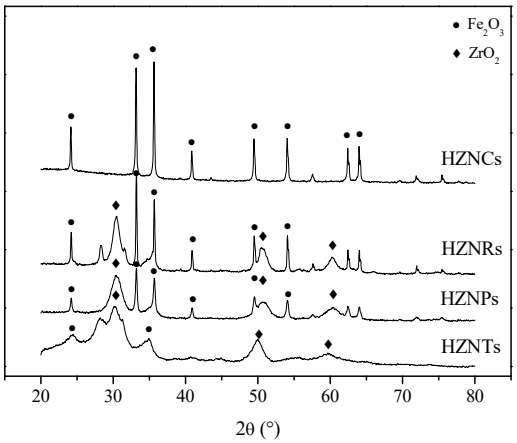

Figure 2. X-ray diffraction (XRD) patterns of the shape-controlled Fe_2O_3–ZrO_2 catalysts.

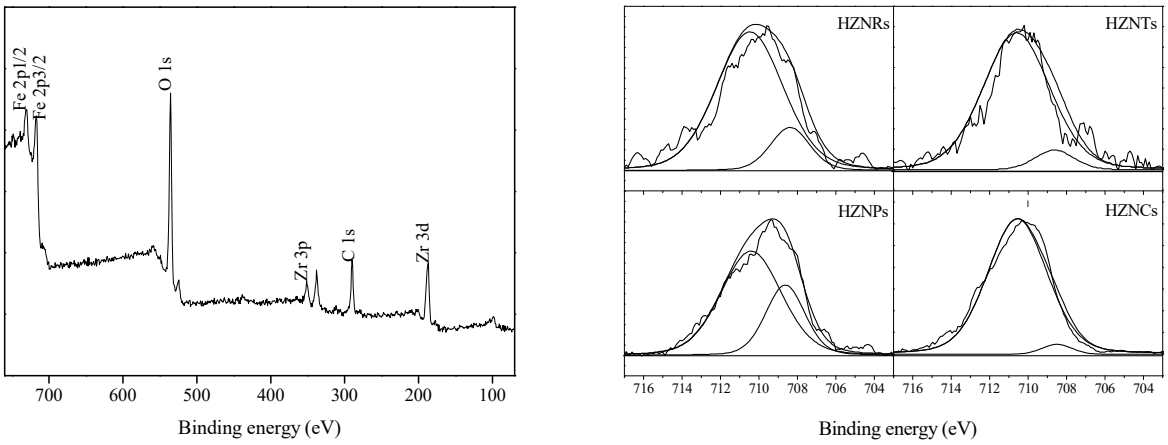

(**a**) (**b**)

Figure 3. X-ray photoelectron spectroscopy (XPS) analysis (**a**) High-resolution spectrum of the HZNPs catalyst. (**b**) Fe $2p_{3/2}$ XPS spectra of the shape-controlled Fe_2O_3–ZrO_2 catalysts.

2.2. The Activity of the Fe_2O_3–ZrO_2 Catalysts

2.2.1. The Interaction of Hematite Facets with H_2O_2

The H_2O_2 adsorption and activation on the catalyst surface are the important steps to produce ·OH radicals and degrade the pollutants in the heterogeneous Fenton-like reaction. High H_2O_2 adsorption could favor the H_2O_2 activation to produce ·OH radicals. Figure 4 shows the H_2O_2 adsorption on the shape-controlled Fe_2O_3–ZrO_2 catalysts at pH 3.0 under 5 °C. The catalysts exhibited

a rapid H_2O_2 adsorption process, and then reached adsorption equilibrium. The order of the H_2O_2 adsorption capacity was HZNPs > HZNRs > HZNCs > HZNTs, and the H_2O_2 adsorption amounts on the catalysts were 45.6, 24.5, 16.3, and 14.3 mg/g_{cat}, respectively. The normalized H_2O_2 adsorption amount per surface area of the Fe_2O_3–ZrO_2 catalysts was calculated, and is shown in Table 2. It was found that HZNPs showed the highest H_2O_2 adsorption capacity (0.43 mg/m^2) which was ca. six times higher than that of HZNTs (0.07 mg/m^2).

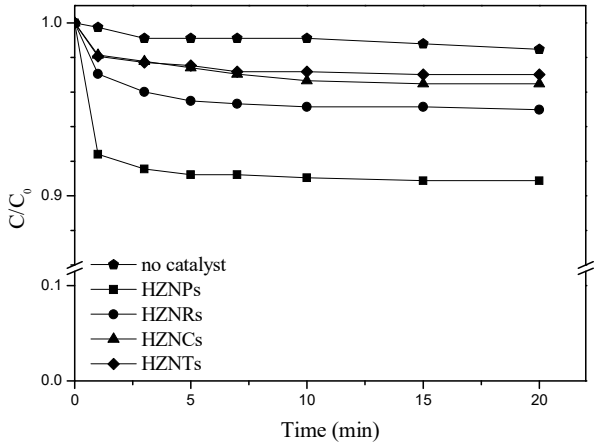

Figure 4. The H_2O_2 absorption on the shape-controlled Fe_2O_3–ZrO_2 catalysts. ([Catalyst] = 0.5 g/L, $[H_2O_2]_0$ = 8 mmol/L, pH = 3, T = 5 °C).

Table 2. H_2O_2 absorption and decomposition properties of the shape-controlled Fe_2O_3–ZrO_2 catalysts.

Sample	A_{H2O2}[a] [mmol/L]	A'_{H2O2}[b] [mg/m²]	B_{H2O2}[c] [%]	k_{H2O2}[d] [min^{-1}]	k_{H2O2}/ Q_{H2O2} [g/(mg·min)]
HZNPs	0.67	0.43	80.1	6.70×10^{-3}	1.47×10^{-4}
HZNRs	0.36	0.25	49.8	3.00×10^{-3}	1.23×10^{-4}
HZNCs	0.21	0.25	37.2	2.00×10^{-3}	1.23×10^{-4}
HZNTs	0.24	0.07	23.5	1.20×10^{-3}	8.40×10^{-5}

[a] H_2O_2 maximum adsorption amount; [b] Adsorption amount of H_2O_2 per unit area; [c] H_2O_2 decomposition rate at 240 minutes; [d] H_2O_2 decomposition rate constant.

The H_2O_2 decomposition on the shape-controlled Fe_2O_3–ZrO_2 catalysts was evaluated at pH 3.0 and a temperature of 45 °C. As shown in Figure 5a, the H_2O_2 decomposition rates of HZNPs, HZNRs, HZNCs, and HZNTs after 240 minute reaction were 80%, 50%, 37%, and 24%, respectively. Moreover, the H_2O_2 decomposition obeyed a pseudo-first kinetic equation (in Figure 5b). The apparent H_2O_2 decomposition rate constants (k_{H2O2}) were 6.70×10^{-3}, 3.00×10^{-3}, 2.00×10^{-3} and 1.20×10^{-3} min^{-1}, and the order was HZNPs > HZNRs > HZNCs > HZNTs, respectively. To further investigate the H_2O_2 decomposition efficiency on the Fe_2O_3–ZrO_2 catalysts, we normalized k_{H2O2} with its maximum adsorption capacity of H_2O_2 (Q_{H2O2}), and the result is shown in Table 2. It was observed that the k_{H2O2}/Q_{H2O2} of HZNPs with a lower surface area had the highest value which was ca. 1.8 times that of HZNTs with a higher surface area. The results indicated that: (1) the H_2O_2 adsorption/decomposition process was related to the morphology, not to the surface area of the Fe_2O_3–ZrO_2 catalysts; (2) a higher adsorption/decomposition on the catalyst surface could be helpful to generate ·OH radicals in the Fenton-like reaction.

In the heterogeneous Fenton-like reaction, the ·OH radicals are known as the main active species for degrading organic compounds. To obtain insight on the ·OH radicals generated on the shape-controlled Fe_2O_3–ZrO_2 catalysts, a quantitative determination was carried out in the presence of H_2O_2 at pH 3.0. For pure Fe_2O_3, there was almost no ·OH formation (not shown), despite a good H_2O_2 adsorption obtained as shown in Figure S2. For the Fe_2O_3–ZrO_2 catalysts, the generated ·OH radicals were detected and the result was shown in Figure 6. The ·OH radicals rapidly increased in the initial 120 minutes reaction, and the concentration was ca. 241.8, 108.8, 72.9, and 35.9 μmol/L for HZNPs,

HZNRs, HZNCs, and HZNTs at 240 minute, respectively. The HZNPs exhibited a higher H_2O_2 decomposition rate and a greater ·OH concentration than the other catalysts. The normalized ·OH concentration per surface area of the catalysts in 240 minute reaction was 4.52, 2.24, 2.20, and 0.37 μmol/m² for HZNPs, HZNRs, HZNCs, and HZNTs, respectively. The normalized ·OH amount of HZNPs was ca. 12 times that of HZNTs. The results further confirmed that the ·OH generation was independent of the specific surface area and was mainly affected by the morphologies of the Fe_2O_3–ZrO_2 catalysts. In addition, the free ·OH radicals generated were the main chemical state for total ·OH radicals in the Fenton-like reaction (in Figure S3). The shape-controlled Fe_2O_3–ZrO_2 catalysts favored the free ·OH formation when they reacted with H_2O_2. It was found that the free ·OH concentration for all catalysts was obviously higher than that of the SMT in the solution, indicating that the desorption of the generated ·OH radicals from the catalyst surface was not a limiting step for the SMT degradation in our experiments.

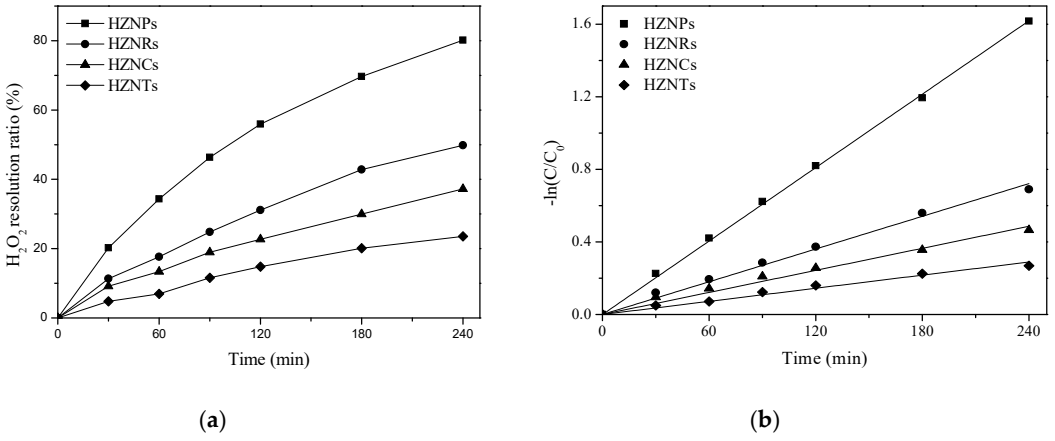

Figure 5. The H_2O_2 decomposition and decomposition kinetics curves on the shape-controlled Fe_2O_3–ZrO_2 catalysts (**a**) H_2O_2 decomposition curves; (**b**) H_2O_2 decomposition kinetics curves ([Catalyst] = 0.5 g/L, $[H_2O_2]_0$ = 8 mmol/L, pH = 3, T = 45 °C).

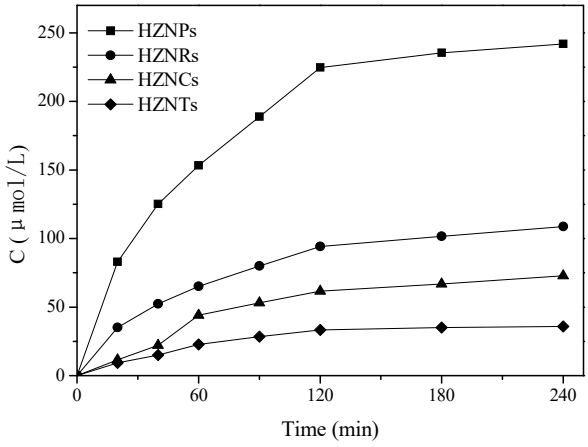

Figure 6. Quantitative determination of ·OH radicals generated by the shape-controlled Fe_2O_3–ZrO_2 catalysts in the presence of H_2O_2. ([Catalyst] = 0.5 g/L, $[H_2O_2]_0$ = 8 mmol/L, pH = 3, T = 45 °C).

2.2.2. The Activity of the Fe_2O_3–ZrO_2 Catalysts

The Fenton-like reaction degrading the SMT was conducted at pH 3.0 and with an initial SMT concentration of 10 mg/L over the shape-controlled Fe_2O_3 and Fe_2O_3–ZrO_2 catalysts (see Figure S4 and Figure 7a). In the H_2O_2 and Fe_2O_3/H_2O_2 systems, almost no SMT removal was obtained after 240 minutes, indicating that both systems were not active for removing SMT. In the heterogeneous Fe_2O_3–ZrO_2/H_2O_2 system, the SMT removal significantly increased, while the SMT adsorption on the Fe_2O_3–

ZrO_2 catalysts was negative (<5%). The result indicated that the shape-controlled Fe_2O_3–ZrO_2 catalysts exhibited good activity in the Fenton-like reaction of the SMT degradation. Moreover, the activity order was as follows: HZNPs > HZNRs > HZNCs > HZNTs, and HZNPs exhibited the best catalytic activity, whose SMT removal reached 98% after 240 minutes.

As shown in Figure 7b, a pseudo-first kinetic equation was obtained in the Fenton-like reaction for the SMT degradation over the shape-controlled Fe_2O_3–ZrO_2 catalysts. The apparent rate constants (k) for HZNPs, HZNRs, HZNCs, and HZNTs were 1.5×10^{-2}, 6.8×10^{-3}, 1.7×10^{-3}, and 9.3×10^{-4} min^{-1}, respectively. We normalized the rate constant (k) with the surface area of the Fe_2O_3–ZrO_2 catalysts. The value of HZNPs (1.4×10^{-4} g × min^{-1} × m^{-2}) was the highest, which was ca. two times that of HZNRs (7.0×10^{-5} g × min^{-1} × m^{-2}) and ca. 29 times that of HZNTs (4.8×10^{-6} g × min^{-1} × m^{-2}). The results indicated that the activity of the shape-controlled Fe_2O_3–ZrO_2 catalysts was closely related to the morphology, not the surface area of the catalysts.

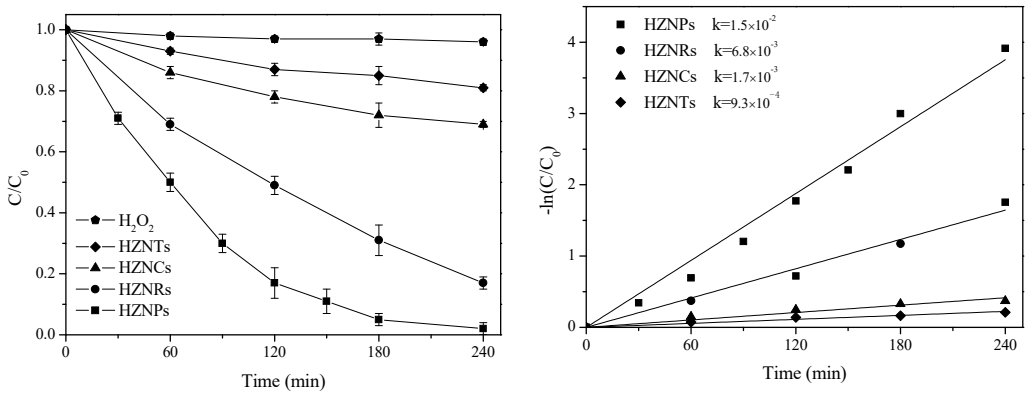

(**a**) (**b**)

Figure 7. The sulfamethazine (SMT) removal efficiency and SMT removal kinetics curves in the Fenton-like reaction over the shape-controlled Fe_2O_3–ZrO_2 catalysts (**a**) SMT removal efficiency. (**b**) SMT removal kinetics. ([Catalyst] = 0.5 g/L, $[H_2O_2]_0$ = 8 mmol/L, pH = 3, T = 45 °C).

During the Fenton-like reaction, the Fe ion leaching was measured after 240 minutes, and a low concentration of Fe ion leaching was obtained (<0.2 mg/L). The results indicated that the Fe_2O_3–ZrO_2 catalysts had good stability in the Fenton-like reaction for degrading SMT. The intermediates for the SMT degradation over HZNPs were detected by liquid chromatography–mass spectrometry (LC–MS). Several main intermediate products were obtained, including 4-amino-N-carbamimidoyl-benzenesulfonamide, 4,6-dimethyl-2-hydroxypyrimidine, sulfanilamide, aniline, and carboxylic acid, in good agreement with the literature [21].

2.3. Mechanism Analysis

In the heterogeneous Fenton-like reaction, the H_2O_2 adsorption and the H_2O_2 activation on the catalyst surface were the key steps limiting ·OH generation. In the literature [22], the adsorption of atoms, ions, and molecules on a catalyst surface is related to their morphologies, that is, the intrinsic crystal structure. For iron-based catalysts, the substance adsorption was both related to the exposed facets and the surface densities of the iron atoms (SDIAs) [13,17]. In our study, the order of the H_2O_2 adsorption on pure Fe_2O_3 was nanorods > nanoplates > nanocubes > nanotubes (see Figure S2), in agreement with the above result. With the Zr addition, the SDIAs decreased (in Table 1), and led to a decrease of H_2O_2 adsorption on the Fe_2O_3–ZrO_2 catalysts (in Figure 4). It was noticed that HZNPs and HZNRs showed an obvious change in H_2O_2 adsorption. For Fe_2O_3 nanoplates and nanorods, the main {001} and exposed {110} facets could adsorb the substances on the catalyst surface, and {110} facets had a higher reactivity than {001} facets in the adsorption process [13]. This suggested that Fe_2O_3 nanorods exhibited a better adsorption capacity than Fe_2O_3 nanoplates. Therefore, Zr ions, as

foreign substances, could be easily confined on the Fe_2O_3 nanorods, indicating that more Zr ions occupied the exposed facet of HZNRs. This result led to the decrease of the SDIAs on the HZNRs. HZNPs exhibited a better H_2O_2 adsorption capacity than HZNRs.

Another key step limiting the ·OH generation, H_2O_2 activation, had a close relationship with the Fe^{2+} amount on the surface for the iron-based catalysts in the Fenton-like reaction [16]. The Zr addition obviously increased the surface area and induced the presence of Fe^{2+} on the catalyst surface. Moreover, the Fe^{2+} density site (Fe^{2+}/nm^2) of the Fe_2O_3–ZrO_2 catalysts (see Table 1) showed a closed relationship with the morphologies of the catalysts, rather than the surface areas. HZNPs with a low surface area had the highest Fe^{2+} site density, suggesting that the morphology affected the Fe^{2+} density sites on the surface of the Fe_2O_3–ZrO_2 catalysts.

In the heterogeneous Fenton-like system for degrading organic compounds, a radical chain reaction is commonly involved [2,5,6,16]. In our study, there were important reaction processes for ·OH radical generation, as follows. First, the H_2O_2 adsorption was the first step for the H_2O_2 activation to ·OH radicals on the catalyst surface. A higher H_2O_2 adsorption was helpful to react with Fe^{2+} on the catalysts and produce ·OH radicals. Second, the H_2O_2 activation occurred according to the reaction between $\equiv Fe^{2+}$ with the adsorbed H_2O_2 by electron transfer (Equation 1). The result suggested that the ·OH radical formation was attributed to the H_2O_2 adsorption and Fe^{2+} density sites on the Fe_2O_3–ZrO_2 catalysts. Then the ·OH radicals, adsorbed on the surface by weak chemical bonds, easily desorbed to the free ·OH radicals in the solution, and rapidly oxidized organic pollutants. In the Fenton-like reaction, ZrO_2 with an amorphous and small particle on the catalyst surface, enhanced the regeneration process of $\equiv Fe^{2+}$ from $\equiv Fe^{3+}$ in the presence of H_2O_2 at a low pH value (Equations 2, 3 and 4) [16]. Therefore, in the Fenton-like reaction process over the Fe_2O_3–ZrO_2 catalysts, the higher H_2O_2 adsorption and Fe^{2+} density sites favored greater ·OH generation. The result suggested that HZNPs exhibited the best SMT removal, due to the highest H_2O_2 adsorption and Fe^{2+} density sites.

$$\equiv Fe^{2+} + H_2O_2 \rightarrow \equiv Fe^{2+}\text{-}H_2O_2 \rightarrow \equiv Fe^{3+} + \cdot OH + OH^- \quad (1)$$

$$\equiv Fe^{3+} + H_2O_2 \rightarrow \equiv Fe^{2+} + O_2\cdot^-/HO_2\cdot + H^+ \quad (2)$$

$$\equiv Fe^{3+} + O_2\cdot^-/HO_2\cdot \rightarrow \equiv Fe^{2+} + O_2 + H^+ \quad (3)$$

$$\equiv Zr\text{-}HO_2^- + H_2O_2 \rightarrow OH\cdot + \equiv Zr^+\text{-}O_2\cdot^- + H_2O \quad (4)$$

3. Materials and Methods

3.1. Materials and Chemicals

In the experiments, chemical reagents without further purification were obtained from Aladdin Industrial Corporation in China. Methanol, acetic acid, and H_2O_2 (30 wt.%) were purchased from the Sigma-Aldrich Company.

3.2. Synthesis Methods

Fe_2O_3 and Fe_2O_3–ZrO_2 catalysts were prepared by the hydrothermal method according to the literature [17,18]. The Fe to Zr atomic ratio was one.

3.2.1. Preparation of Fe_2O_3–ZrO_2 and Fe_2O_3 Nanoplates

Amounts of 1.092 g of $FeCl_3 \times 6H_2O$ and 1.289 g of $ZrOCl_2 \times 8H_2O$ were dissolved in ethanol (40 mL) with a trace addition of distilled water (2.8 mL) under vigorously stirring. Sodium acetate (3.2 g) was added under stirring for 1 hour. Then, the mixture was sealed in a Teflon-lined stainless steel autoclave (Kenuo, Beijing, China, 100 mL) and maintained at 180 °C for 12 hours. After natural cooling to room temperature, the resulting solid was washed with distilled water and ethanol several times to remove any impurities and dried at 100 °C overnight. Finally, the products were ground and

calcined at 500 °C for 3 hours under air to obtain HZNPs. Pure Fe_2O_3 nanoplates (HNPs) were prepared in a similar way.

3.2.2. Preparation of Fe_2O_3–ZrO_2 and Fe_2O_3 Nanorods

Amounts of 1.683 g of $Fe(NO_3)_3 \times 9H_2O$ and 1.788 g of $Zr(NO_3)_4 \times 5H_2O$ were dissolved in 45 mL of deionized water. After completely dissolving, NaOH solution (10 wt.%) was added dropwise to adjust the pH to 12 ± 0.1, and then the mixture was vigorously stirred for 30 minutes. The mixture was transferred into a Teflon-lined stainless steel autoclave (100 mL) and kept at 180 °C for 12 hours. After washing and drying the precipitate as in the previous method, the solid was calcined at 500 °C for 3 hours under air to obtain HZNRs. Pure Fe_2O_3 nanorods (HNRs) were prepared in a similar way.

3.2.3. Preparation of Fe_2O_3–ZrO_2 and Fe_2O_3 Nanocubes

Amounts of 0.811 g of $FeCl_3 \times 6H_2O$ and 1.288 g of $Zr(NO_3)_4 \times 5H_2O$ were dissolved in 50 mL of cetrimonium bromide (CTAB) aqueous solution (C_{CTAB} = 0.04 mol/L) under vigorous stirring for 30 minutes, and then transferred into a Teflon-lined stainless steel autoclave (100 mL) and maintained at 120 °C for 12 hours. After washing and drying the precipitate as in the previous method, the solid was calcined at 500 °C for 3 hours under air to obtain HZNCs. Pure Fe_2O_3 nanocubes (HNCs) were prepared in a similar way.

3.2.4. Preparation of Fe_2O_3–ZrO_2 and Fe_2O_3 Nanotubes

Amounts of 1.081 g of $FeCl_3 \times 6H_2O$ and 1.289 g of $ZrOCl_2 \times 8H_2O$ were dissolved in 60 mL of $NH_4H_2PO_4$ solution ($C_{NH_4H_2PO_4}$ = 0.04 mol/L). After stirring for 30 minutes, the mixture was transferred into a Teflon-lined stainless steel autoclave (100 mL) and kept at 220 °C for 12 hours. After washing and drying as in the previous method, the solid was calcined at 500 °C for 3 hours under air to obtain HZNTs. Pure Fe_2O_3 nanotubes (HNTs) were prepared in a similar way.

3.3. Catalyst Characterization

The morphology of the catalysts was obtained by a Hitachi SU8010 field emission scanning electron microscope (FESEM) (Hitachi,Tokyo, Japan) using an accelerating voltage of 5 kV. The specific surface area of the catalysts was measured by N_2 adsorption at 77 K using an Autosorb iQ-MP system (Quantachrome Instruments, Boynton Beach, Florida, USA). Before analysis, the sample was outgassed at 200 °C for 4 hours. The X-ray diffraction (XRD) pattern of the catalysts was measured on a Bruker D8 Focus diffractometer (Bruker, Karlsruher, Germany) using Cu Kα radiation (λ = 0.15406 nm). X-ray photoelectron spectroscopy (XPS) analysis for the catalysts was performed on a PHI 5400 ESCA analyser with an Al Kα X-ray source (PHI, Chanhassen, MN, USA) (hν = 1486.60 eV). The C1s peak (E_b = 284.60 eV) was used as a reference for the calibration of the binding energy.

3.4. H_2O_2 and ·OH Concentration Measurement

Titanium oxalate spectrophotometry was used for detecting the H_2O_2 concentration in the Fenton reaction. The concentration of hydroxyl radicals (·OH) was analyzed with a modified methanol probe molecule method [23]. Hydroxyl radicals reacted with methanol to form formaldehyde, and then the formaldehyde was determined by the 2,4-dinitrophenylhydrazine (DNPH) derivation method. The concentration of DNPH–formaldehyde derivative was measured by high-performance liquid chromatography (HPLC, Agilent 1260, Agilent, Santa Clara, CA, USA) with a C18 column at 400 nm.

3.5. Fenton Degradation Experiments

The experiments were performed in a 500 mL glass flask in the dark, equipped with a stirrer and a thermocouple. First, the initial pH of the SMT solution was adjusted to 3.0 ± 0.05 by adding 5 wt.% HCl, and then a catalyst and an SMT solution (10 mg/L, 250 mL) were loaded into the reactor with stirring. The reactor was heated to 45 °C, and then maintained for 30 minutes to achieve adsorption equilibrium on the catalyst. Secondly, H_2O_2 was added into the reactor, and the point was defined as "zero" time of the Fenton-like reaction. Samples were periodically withdrawn from the reactor, quenched with methanol, and then filtered through a 0.22 μm filter. The SMT concentration was analyzed by HPLC. The mobile phase was composed of methanol and water (v/v = 60:40). The flow rate was 1.0 mL/min and the detection wavelength was 254 nm.

4. Conclusions

Fe_2O_3–ZrO_2 catalysts with different morphologies were produced successfully by a hydrothermal method. The H_2O_2 adsorption and the Fe^{2+} density sites had a combined effect on ·OH generation in the Fenton-like reaction over the Fe_2O_3–ZrO_2 catalysts. Moreover, the H_2O_2 adsorption and the Fe^{2+} density sites depended on the morphology, rather than the specific surface area. The normalized H_2O_2 adsorption capacity per surface area on the catalyst surface was 0.43 mg/m^2 for HZNPs, and ca. 1.68, 1.72 and 5.75 times that of HZNRs, HZNCs, and HZNTs, respectively. The Fe^{2+} density sites (Fe^{2+}/nm^2) were 5.91, 5.18, 2.44, and 0.90 for HZNPs, HZNRs, HZNCs, and HZNTs, respectively. The normalized ·OH concentration per surface area of the catalysts was 4.52, 2.24, 2.20, and 0.37 μmol/m^2 for HZNPs, HZNRs, HZNCs, and HZNTs, respectively. HZNPs and HZNRs showed a more effective catalytic performance for degrading SMT at pH 3.0 in the Fenton-like reaction. This work indicated that the shape-controlled bimetallic oxides effectively improved the catalytic performance in the heterogeneous Fenton-like reaction.

Supplementary Materials: The following are available online at www.mdpi.com/xxx/s1, Figure S1: XRD patterns of the shape-controlled Fe_2O_3 catalysts, Figure S2: The H_2O_2 absorption with the shape-controlled Fe_2O_3 catalysts, Figure S3: Free ·OH radicals and surface ·OH radicals generated by the shape-controlled Fe_2O_3-ZrO_2 catalysts in the presence of H_2O_2, Figure S4**:** The SMT removal in the Fenton-like reaction over the shape-controlled Fe_2O_3 catalysts, Table S1: Detail information of the shape-controlled Fe_2O_3 catalysts.

Author Contributions: Funding acquisition, P.G. and S.Y.; Investigation, Y.H., Y.S. and M.H.; Project administration, S.Y.; Validation, M.H.; Writing – review and editing, P.G.

Funding: This research received no external funding.

Acknowledgments: The work was supported by National Major Science and Technology Program for Water Pollution Control and Treatment (2017ZX07101-003) and Fundamental Research Funds for Central Universities (2018ZD08, 2018MS033).

Conflicts of Interest: The authors declare no conflict of interest.

References

1. Wang, J.L.; Wang, S.Z. Removal of pharmaceuticals and personal care products (PPCPs) from wastewater: A review. *J. Environ. Manage*. **2016**, *182*, 620–640.
2. Anipsitakis, G.P.; Dionysiou D.D. Radical generation by the interaction of transition metals with common oxidants. *Environ. Sci. Technol*. **2004**, *38*, 3705–3712.
3. Zhao, H.Y.; Qian, L.; Chen, Y.; Wang, Q.N.; Zhao, G.H. Selective catalytic two-electron O_2 reduction for onsite efficient oxidation reaction in heterogeneous electro-Fenton process. *Chem. Eng. J*. **2018**, *332*, 486–496.
4. Xiao, J.D.; Xie, Y.B.; Cao, H.B.; Wang, Y.X.; Guo, Z.; Chen, Y. Towards effective design of active nanocarbon materials for integrating visible-light photocatalysis with ozonation. *Carbon* **2016**, *107*, 658–666.
5. Pereira, M.C.; Oliverira, L.C.A.; Murad, E. Iron oxide catalysts: Fenton and Fenton-like reactions - a review. *Clay Miner*. **2012**, *47*, 285–302.
6. Dhakshinamoorthy, A.; Navalon, S.; Alvaeo, M.; Garcia, H. Metal nanoparticles as heterogeneous Fenton catalysts. *Chem. Sus. Chem*. **2012**, *5*, 46–64.

7. Suanon, F.; Sun, Q.; Li, M.Y.; Cai, X.; Zhang, Y.C.; Yan, Y.J.; Yu, C.P. Application of nanoscale zero valent iron and iron powder during sludge anaerobic digestion: Impact on methane yield and pharmaceutical and personal care products degradation. *J. Hazard. Mater*. **2017**, *321*, 47–53.
8. Wang, Y.B.; Zhao, H.Y.; Zhao, G.H. Iron-copper bimetallic nanoparticles embedded within ordered mesoporous carbon as effective and stable heterogeneous Fenton catalyst for the degradation of organic contaminants. *Appl. Catal. B*. **2015**, *164*, 396–406.
9. Sun, J.Q.; Chen, Y.L.; Chen, J.G. Morphology effect of one-dimensional iron oxide nanocatalysts on Fischer-Tropsch synthesis. *Catal. Sci. Technol*. **2016**, *6*, 7505–7511.
10. Wang, B.H.; Sun, J.Q.; Abbas, M.; Liu, Y.T.; Kong, F.H.; Xiao, H.C.; Chen, J.G. A Novel Hydrothermal Approach for the Synthesis of Flower-Like Fe_2O_3/Fe Foam Nanocrystals and Their Superior Performance in Fisher-Tropsch Synthesis. *Catal. Letter*. **2017**, *147*, 1153–1161.
11. Su, M.H.; He, C.; Shih, K. Facile synthesis of morphology and size-controlled α-Fe_2O_3 and Fe_3O_4 nano-and microstructures by hydrothermal/solvothermal process: The roles of reaction medium and urea dose. *Ceram. Int.* **2016**, *42*, 14793–14804.
12. Hou, L.W.; Zhang, Q.H.; Jérôme, F.; Duprez, D.; Zhang, H.; Royer, S. Shape-controlled nanostructured magnetite-type materials as highly efficient Fenton catalysts. *Appl. Catal. B.* **2014**, *144*, 739–749.
13. Huang, X.P.; Hou, X.J.; Zhao, J.C.; Zhang, L.Z. Hematite facet confined ferrous ions as high efficient Fenton catalysts to degrade organic contaminants by lowering H_2O_2 decomposition energetic span. *Appl. Catal. B.* **2016**, *181*, 127–137.
14. Wan, Z.; Wang, J.L. Degradation of sulfamethazine using Fe_3O_4-Mn_3O_4/reduced graphene oxide hybrid as Fenton-like catalyst. *J. Hazard. Mater*. **2017**, *324*, 653–664.
15. Liang, X.L.; He, Z.S.; Zhong, Y.H.; Tan, W.; He, H.P.; Yuan, P.; Zhu, J.X.; Zhang, J. The effect of transition metal substitution on the catalytic activity of magnetite in heterogeneous Fenton reaction: In interfacial view. *Coll. Surf. A.* **2013**, *435*, 28–35.
16. Gao, P.; Song, Y.; Hao, M.J.; Zhu, A.N.; Yang, H.W.; Yang, S.X. An effective and magnetic Fe_2O_3-ZrO_2 catalyst for phenol degradation under neutral pH in the heterogeneous Fenton-like reaction. *Sep. Purif. Technol.* **2018**, *201*, 238–243.
17. Gao, Q.X.; Wang, X.F.; Di, J.L.; Wu, X.C.; Tao, Y.R. Enhanced catalytic activity of α-Fe_2O_3 nanorods enclosed with {110} and {001} planes for methane combustion and CO oxidation. *Catal. Sci. Technol.* **2011**, *1*, 574–577.
18. Chen, L.Q.; Yang, X.F.; Chen, J.; Wu, J.H.; Zhan, H.Q.; Liang, C.L.; Wu, M.M. Continuous shape- and spectroscopy-tuning of hematite nanocrystals. *Inorg. Chem.* **2010**, *49*, 8411–8420.
19. Wu, W.; Yang, S.L.; Pan, J.; Sun, L.L.; Zhou, J.; Dai, Z.G.; Xiao, X.H.; Zhang, H.B.; Jiang, C.Z. Metal ion-mediated synthesis and shape-dependent magnetic properties of single-crystalline α-Fe_2O_3 nanoparticles. *Cryst. Eng. Comm.* **2014**, *16*, 5566–5572.
20. Scheffe, J.R.; Francés, A.; King, D.M.; Liang, X.H.; Branch, B.A.; Cavanagh, A.S.; George, S.M.; Weimer, A.W. Atomic layer deposition of iron(III) oxide on zirconia nanoparticles in a fluidized bed reactor using ferrocene and oxygen. *Thin Solid Films* **2009**, *517*, 874–1879.
21. Wan, Z.; Wang, J.L. Degradation of sulfamethazine antibiotics using Fe_3O_4–Mn_3O_4 nanocomposite as a Fenton-like catalyst. *J. Chem. Technol. Biot.* **2017**, *92*, 874–883.
22. Wu, C.Z.; Yin, P.; Zhu, X.; OuYang, C.Z.; Xie, Y. Synthesis of hematite (alpha-Fe_2O_3) nanorods: Diameter-size and shape effects on their applications in magnetism, lithium ion battery, and gas sensors. *J. Phys. Chem. B.* **2006**, *110*, 17806–17812.
23. Goldstein, S.; Aschengrau, D.; Diamant, Y.; Rabani, J. Photolysis of aqueous H_2O_2: Quantum yield and applications for polychromatic UV actinometry in photoreactors. *Environ. Sci. Technol.* **2007**, *41*, 7486–7490.